Geometry of the nuclear envelope determines its flexural stiffness

Ashutosh Agrawal[a,*] and Tanmay P. Lele[b]
[a]Department of Mechanical Engineering, University of Houston, Houston, TX 77204; [b]Department of Biomedical Engineering and Department of Chemical Engineering, Texas A&M University, College Station, TX 77843

ABSTRACT **During closed mitosis in fission yeast, growing microtubules push onto the nuclear envelope to deform it, which results in fission into two daughter nuclei. The resistance of the envelope to bending, quantified by the flexural stiffness, helps determine the microtubule-dependent nuclear shape transformations. Computational models of envelope mechanics have assumed values of the flexural stiffness of the envelope based on simple scaling arguments. The validity of these estimates is in doubt, however, owing to the complex structure of the nuclear envelope. Here, we performed computational analysis of the bending of the nuclear envelope under applied force using a model that accounts for envelope geometry. Our calculations show that the effective bending modulus of the nuclear envelope is an order of magnitude larger than a single membrane and approximately five times greater than the nuclear lamina. This large bending modulus is in part due to the 45 nm separation between the two membranes, which supports larger bending moments in the structure. Further, the effective bending modulus is highly sensitive to the geometry of the nuclear envelope, ranging from twofold to an order magnitude larger than the corresponding single membrane. These results suggest that spatial variations in geometry and mechanical environment of the envelope may cause a spatial distribution of flexural stiffness in the same nucleus. Overall, our calculations support the possibility that the nuclear envelope may balance significant mechanical stresses in yeast and in cells from higher organisms.**

Monitoring Editor
Dennis Discher
University of Pennsylvania

Received: Mar 2, 2020
Revised: Jun 1, 2020
Accepted: Jun 10, 2020

INTRODUCTION

Intranuclear microtubule elongation during closed mitosis in the fission yeast *Schizosaccharomyces pombe* generates pushing forces on the nuclear envelope (West *et al.*, 1998; Zheng *et al.*, 2007). These forces deform the initially spherical nucleus into ellipsoidal and then dumbbell shapes, finally ending in nuclear fission into two daughter nuclei. Because yeast lack a lamin-like structure, mechanical stresses associated with bending and in-plane extension of the nuclear envelope likely balance the forces of microtubule elongation during close mitosis. For example, a computational model accounting for microtubule forces and nuclear envelope mechanics has been used to predict nuclear shape transformations typical of closed mitosis (Lim *et al.*, 2007). Deformation of the yeast nuclear envelope also helps balance forces due to cytoplasmic microtubule polymerization that position the nucleus (Tran *et al.*, 2001). In all these situations, the extent to which the nuclear envelope deforms depends on its flexural stiffness, but the stiffness of the envelope is currently unknown. In addition to its obvious importance in yeast, envelope mechanics may be important in other contexts. For example, mammalian stem cells lack nuclear lamins. As such, any mechanical stresses on the stem cell nucleus must be balanced at least in part by the envelope. In confined cell migration, the nuclear envelope separates from the lamina and the nucleoplasm, forms blebs, and then ruptures (Denais *et al.*, 2016; Halfmann *et al.*, 2019; Warecki *et al.*, 2020). The flexural stiffness of the envelope likely plays an important role in determining the stress distribution in the membranes during this process and may be important in the subsequent mechanics of repair.

This article was published online ahead of print in MBoC in Press (http://www.molbiolcell.org/cgi/doi/10.1091/mbc.E20-02-0163) on June 17, 2020.

*Address correspondence to: Ashutosh Agrawal (ashutosh@uh.edu).

Abbreviations used: INM, inner nuclear membrane; LINC complex, linker of nucleoskeleton and cytoskeleton complex; NPC, nuclear pore complex; ONM, outer nuclear membrane.

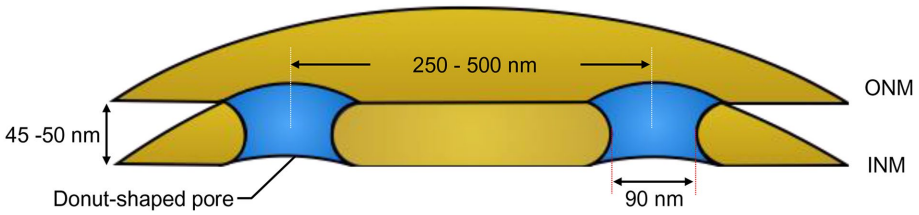

FIGURE 1: Geometry of the nuclear envelope. The outer nuclear membrane (ONM) and the inner nuclear membrane (INM) are fused together at donut-shaped pores with an average diameter of 90 nm. The membranes are maintained at an average separation of 45–50 nm. The spacing between adjacent pores is 250–500 nm.

The nuclear envelope is not a single membrane, but comprises the outer nuclear membrane (ONM) and the inner nuclear membrane (INM), which are fused at donut-shaped pore sites (Figure 1; see also Figure 1 in Otsuka *et al.*, 2016). The bending modulus of the double-membrane envelope is expected to be higher than that of the single membrane, but predicting its value is not trivial. The bending modulus of a thin film scales with the cube of its thickness (Landau and Lifshitz, 1986); however, this scaling is valid for a film in which the layers cannot slide past each other and also is valid only for continuum materials where the thickness is much larger than molecular size and not for liquids that exhibit quadratic scaling (Bermúdez *et al.*, 2004). In contrast, the ONM and the INM can slide past each other. As such, models of nuclear envelope mechanics have typically assumed that the bending modulus of the envelope is twice that of a single lipid membrane (Vaziri *et al.*, 2006; Lim *et al.*, 2007; Vaziri and Mofrad, 2007). A similar assumption has been made in models of membranes adherent to each other in other contexts (Deserno *et al.*, 2007; Agrawal, 2011; Yi *et al.*, 2011). Such an assumption may be inapplicable to the nuclear envelope given the fact that the two nuclear membranes are spaced ~30–50 nm apart (Franke *et al.*, 1981). This spacing may cause the bending modulus of the envelope to be even larger than current estimates (Deviri *et al.*, 2017). Furthermore, the two membranes are also fused at pores spaced at 250–500 nm (Belgareh and Doye, 1997; D'Angelo *et al.*, 2006; Dultz and Ellenberg, 2010), which can in turn impact the flexural stiffness of the nuclear envelope.

Here we used computational modeling to analyze the deformation of a patch consisting of two membranes fused at a donut-shaped pore under an applied force. We tested two hypotheses: 1) the resistance to bending deformations of the nuclear envelope, that is, its flexural stiffness, defined as the ratio of the applied force to the displacement undergone at the point of application of the force (units of pN/nm), is higher than that of a single lipid membrane, and 2) the flexural stiffness of the envelope depends on the spacing between the constituent membranes of the envelope and on the distance between adjacent pores. We used the calculations to estimate the effective bending modulus of a single membrane with a hole. The effective bending modulus accounts for the material property of the membrane and the cross-sectional geometry of the double-membrane system (units of pN nm) and is independent of the size of the membrane or the nature of the applied force on the membrane. Our calculations show that the effective bending stiffness and bending modulus of a membrane patch consisting of two membranes fused at a pore are more than one order of magnitude higher than that of a single membrane. These properties are sensitive to the spacing between the membranes and the interpore separation distance.

RESULTS

Mechanics of a single membrane

We modeled a patch of membrane under force as a homogeneous two-dimensional (2D) elastic surface that resists bending deformations and is inextensible. The internal energy of the membrane was defined by the Helfrich–Canham energy (Eq. 1 Canham, 1970; Helfrich, 1973; Jenkins, 1977; Steigmann, 1999). We solved the Euler–Lagrange equation along with geometric equations (Eq. 3) to calculate membrane shapes under a locally applied tensile force F. We computed force-displacement curves and computed the effective flexural stiffness as the slope of this curve at low displacements where the force-displacement relationship is linear.

Our goal was to compare the mechanical behavior of a single-membrane patch with that of two-membrane patches joined together at a pore. As such, we first calculated the shape of a single axisymmetric membrane patch with or without a pore in it, under applied force (Figure 2, A and B). In the next section, we assume a pore-to-pore separation of 350 nm. We therefore set the radius of the single-membrane patch at 175 nm for comparative purposes (Figure 2A). We numerically solved the Euler–Lagrange equations (Eq. 3) for appropriate boundary conditions (see *Methods Model* section for details). For the patch without a pore, the membrane is assumed to be locally flat at the center point where a point force is applied. For the patch with a pore, the membrane is assumed to rotate freely at the inner boundary (i.e., at a radius of 45 nm). The membrane shape far away from the point of force application for both patches was assumed to be unperturbed from its original resting flat shape (Figure 2A). As a check on the numerical calculations, we compared them with analytical solutions for the shape of the axisymmetric membrane under force calculated from the linearized Euler–Lagrange equations (Eq. 4).

Typical examples of an analytical solution (solid blue) of the linearized Euler–Lagrange equations and numerical solutions (dashed cyan) of the nonlinear Euler–Lagrange equations for the membrane patches in Figure 2, A and B, are shown in Figure 2C (the maximum displacement in the solutions is 5 nm). The analytical solutions and numerical solutions are in good agreement with each other for both types of patches (Figure 2C). Both linear and nonlinear calculations predicted a linear force-displacement relationship, again in good agreement with each other (Figure 2D). The slope of the force-displacement curve yielded an effective stiffness F/z_{max} of the membrane patch without a pore of ~0.13 pN/nm (meaning that a tensile force of 0.13 pN is required for every nanometer deflection of the center of the membrane patch) and an effective stiffness of 0.16 pN/nm for the membrane patch with a pore. These calculations validate our numerical method, which we next used for computing the mechanics of two membranes fused together at a pore.

Mechanics of two membranes fused at a pore

Analytical calculations are not feasible for the two-membrane system owing to its complex geometry (Figure 1). As such, we simulated a unit cell of the nuclear envelope that consisted of two membrane patches each of radius ~175 nm fused at a single donut-shaped pore of radius 45 nm (Figure 3A). The separation between membranes far away from the pore was fixed at 45 nm (Franke *et al.*, 1981). One boundary condition imposed a fixed pore radius while allowing membranes there to rotate and translate freely in the vertical direction. To maintain the separation between membranes at

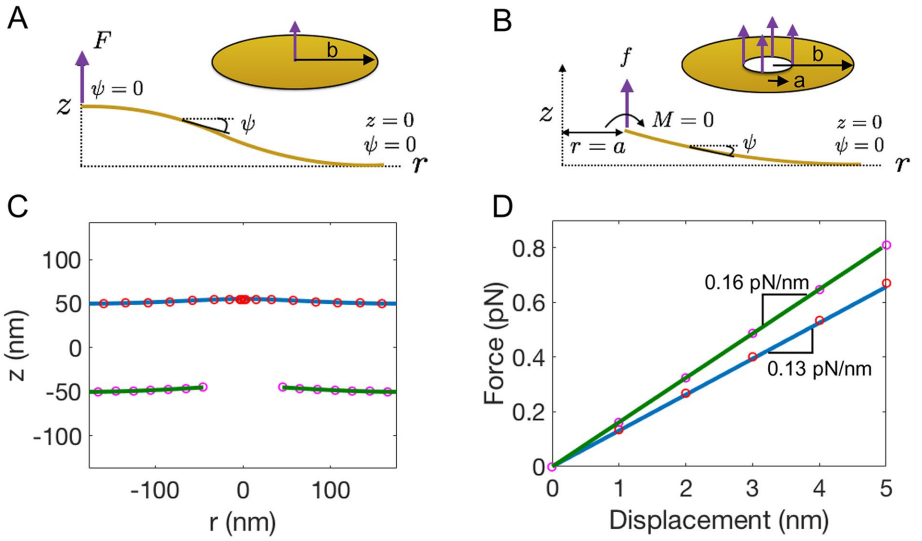

FIGURE 2: Calculations of the mechanics of a single-membrane patch. (A) A single membrane of radius 175 nm is subjected to an upward-acting point force at the center. Schematic shows the boundary conditions for the model. At the center ($r = 0$), the membrane is required to be locally flat and the applied force is equal to F. At the outer boundary ($b = 175$ nm), the membrane is required to be flat and have zero height. (B) A single membrane with a pore of radius 45 nm (outer radius is 175 nm) is subjected to an upward-acting point force at the inner boundary. Schematic shows the boundary conditions for the model. At the inner boundary ($a = 45$ nm), the membrane is free to rotate and the applied force is equal to F. At the outer boundary ($b = 175$ nm), the membrane is required to be flat and have zero height. (C) The cross-section of the membranes under force calculated analytically (solid blue and green lines) and numerically (red and magenta circles) at a maximum displacement of 5 nm. (D) Force-displacement plots calculated from analytical (solid blue and green lines) and numerical calculations (red and magenta circles). The slopes of the lines are ~0.13 and 0.16 pN/nm for the membranes with no pore and pore, respectively. These are the effective stiffnesses of the two single-membrane systems.

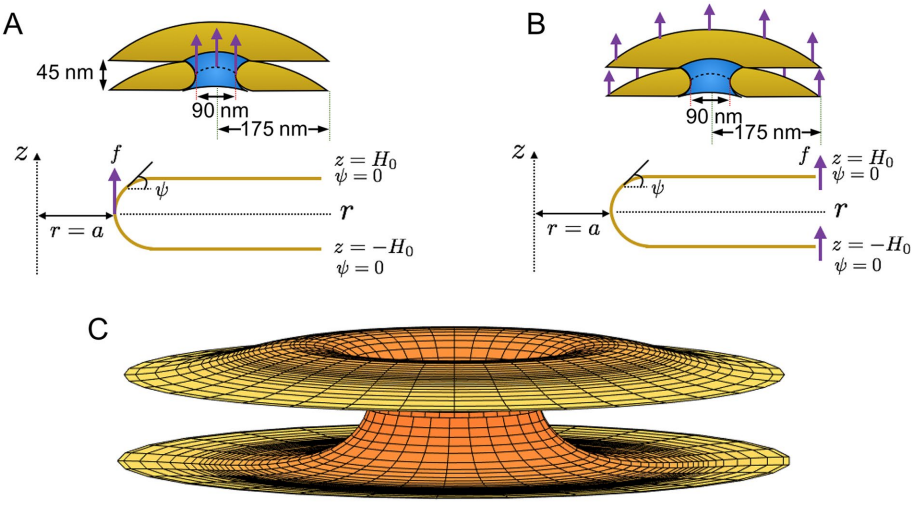

FIGURE 3: Force application on two membrane patches fused together. (A) Geometry of the nuclear membranes fused at the donut pore under an applied force at the equatorial ring. The schematic shows the geometric quantities and the boundary conditions employed to compute the force-deformation response. The boundary conditions correspond to Eq. 3 in the *Methods* section. At the inner boundary, the radius is fixed at 45 nm ($a = 45$ nm) and the total applied force is equal to F. At the outer boundary ($b = 175$ nm), the two membranes have zero slope with a height equal to half the separation distance between the ONM and INM ($H_0 = 22.5$ nm) below and above the reference plane ($z = 0$). (B) The system in A is subjected to force at the outer boundary of both the membranes. The total vertical force acting on the two membranes is equal to F. (C) Calculated three-dimensional geometry of the model in A under a force of 7.13 pN and no imposed in-plane tension.

45 nm away from the pore, the other boundary condition prescribed the vertical height of the membrane above the line of symmetry and required the membrane to be flat (clamped support) far away from the pore (Figure 3B).

Membranes at nuclear pores typically tend to be flat and at a regular distance from each other (Ogawa-Goto *et al.*, 2003). We have previously shown that a flat shape near the pore necessitates prescription of tension in a membrane lacking curvature-inducing proteins (Torbati *et al.*, 2016). To ensure that the membrane was flat near the pore, in one calculation we imposed a modest in-plane tension of 0.2 mN/m in the membrane (Torbati *et al.*, 2016), while in another, we set the tension to zero. We applied force on an equatorial ring of the pore (Figure 3A) and integrated the set of nonlinear Euler–Lagrange equations numerically to compute the geometry of the two-membrane system. Figure 3C shows a typical example of the calculated three-dimensional solution under an applied force of 7.13 pN on the equatorial ring (in-plane tension in this example was set to zero). Because the geometry is axisymmetric, it is sufficient to examine the vertical cross-section of the geometry.

We quantified the vertical displacement of the equatorial plane and plotted the force-displacement relationships of two-membrane patches under in-plane tension (purple), two-membrane patches under zero in-plane tension (yellow), and a single-membrane patch with a pore under zero in-plane tension (green) (Figure 4A). We applied force over the equatorial ring of the pore for the two-membrane calculations (Figure 3A) and over the circumference of the pore for the case of the single membrane (Figure 2B). The force–displacement curves for both two-membrane patches were substantially different from that of the single membrane. The force-displacement relationship deviated from linearity at larger force magnitudes for the two-membrane patches at zero tension. Figure 4B shows calculated cross-sections of the three systems (same color coding as Figure 4A), each at a maximum vertical displacement of 5 nm.

By analogy with the analytical solution for the single membrane with a pore, we computed the effective stiffness F/z_{max} for the two-membrane patch as the slope of the initial linear region of the force-displacement curves in Figure 4A; Figure 4B shows the corresponding shapes of the membrane system. The flexural stiffness of the fused membranes with and without tension was found to be ~1.65 pN/nm, which is more

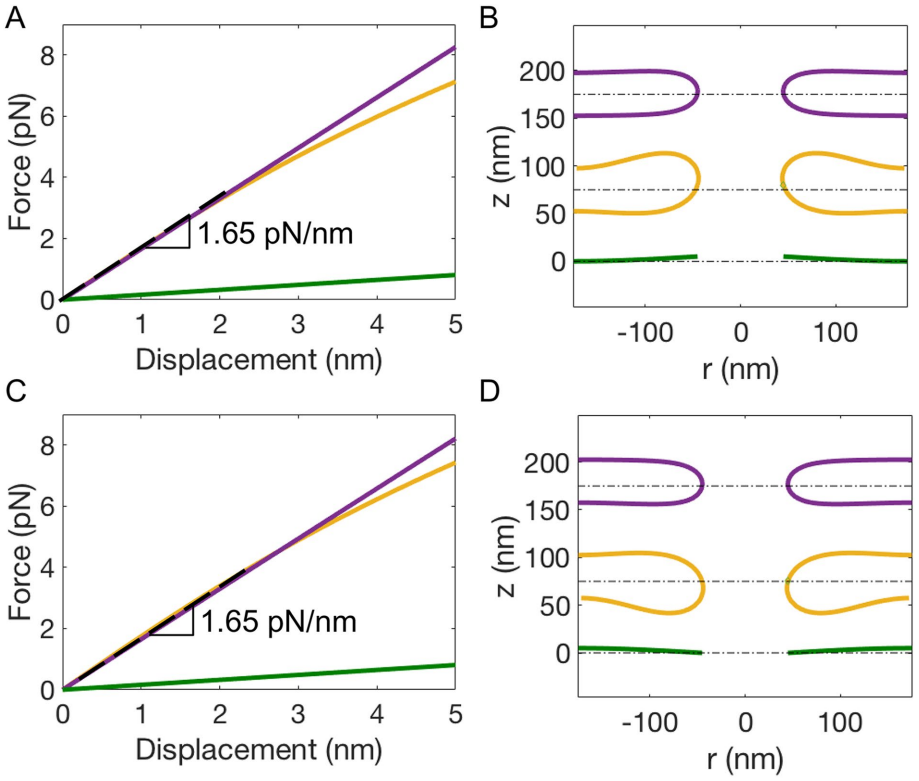

FIGURE 4: Mechanical response of the two-membrane patch. (A) Force-displacement plots of the two-membrane system depicted in Figure 3A under a prescribed in-plane tension of 0.2 mN/m (purple curve) and zero in-plane tension (yellow curve). The two curves have approximately the same initial slope of 1.65 pN/nm, which is ~10 times the slope of the single membrane with a pore of 0.16 pN/nm (green curve). (B) The cross-section of the three systems at 5 nm displacement (color coding corresponds to that in A). (C) Force-displacement plots of the two-membrane system depicted in Figure 3B under a prescribed in-plane tension of 0.2 mN/m (purple curve) and zero in-plane tension (yellow curve). The two curves again show an initial slope ~10 times the slope of the single membrane with a pore (green curve). (D) The cross-section of the three systems at 5 nm displacement (color coding corresponds to that in C).

than an order of magnitude larger than that of the single membrane with a pore (0.16 pN/nm).

As modeling studies typically model the envelope as a single membrane with an effective bending stiffness, we can approximate the two-membrane patch with an equivalent single-membrane system with the same outer radius (i.e., 175 nm). Because the bending stiffness k_h is proportional to the bending modulus k ($k_h = \frac{k}{\beta_h}$, where β_h is a factor accounting for the size and the boundary conditions of the membrane; see Eq. 12 in the *Model* section), the effective bending modulus of the two-membrane patch for the estimated bending stiffness of 1.65 pN/nm is ~1700 pN/nm, which is an order of magnitude larger than the modulus of a single membrane of ~165 pN/nm (see Table 1).

To further test the robustness of our predictions, we set the force at the equator to zero and instead applied it to the outer boundary of the double-membrane domain and computed the effective bending moduli. Changing the location of the force in this manner did not have any noticeable impact on the flexural stiffness (Figure 4, C and D). Since the stiffness is unchanged for two distinct forcing scenarios (force applied at the inner and force applied at the outer boundary), we conclude that the calculated flexural stiffness is generally valid for the double-membrane patch.

Effect of geometry on envelope mechanics

The calculations above showed that two-membrane patches fused at donut-shaped holes are significantly stiffer to bending than single membranes. To examine the reasons for this, we varied the geometry of the membrane patches and quantified the effect on effective flexural stiffness. Specifically, we examined the effect of 1) distance of separation between the membranes, 2) pore-to-pore separation (meaning membrane patch radius), and 3) pore radii, on stiffness.

Calculations of force-displacement curves along with examples of membrane shapes at displacements of 5 nm are shown in Figure 5. In these calculations, force was applied at the equatorial ring and the in-plane tension was set to zero. The initial slope of the force-displacement curves varied directly as the separation between membranes (Figure 5) and the pore radius (Figure 5, A and E), and it varied inversely as the pore-to-pore separation (Figure 5C; the numerical value of flexural stiffness is marked as the slope of the force-displacement curves in Figure 5). At large displacements of 5 nm, the slopes tended to decrease but remained significantly larger than for the single membrane.

Motivated by the above calculations, we hypothesized that the stiffness of the double-membrane system should approach that of two single membranes in close apposition upon reducing the pore diameter and the membrane spacing to their minimum value. Interestingly, the flexural stiffness was found to be ~0.3 pN/nm

System	Bending modulus (pN/nm)	Reference
Single membrane	165	Boal and Boal, 2012
Two-membrane model with geometry in Figure 3A	1700	This study
Nuclear envelope modeled as a single membrane	400	Lim *et al.*, 2007
	360	Vaziri *et al.*, 2006
	200	Vaziri and Mofrad, 2007
Nuclear lamina	350	Vaziri *et al.*, 2006; Vaziri and Mofrad, 2007

TABLE 1: Bending moduli of membranes and the nuclear lamina.

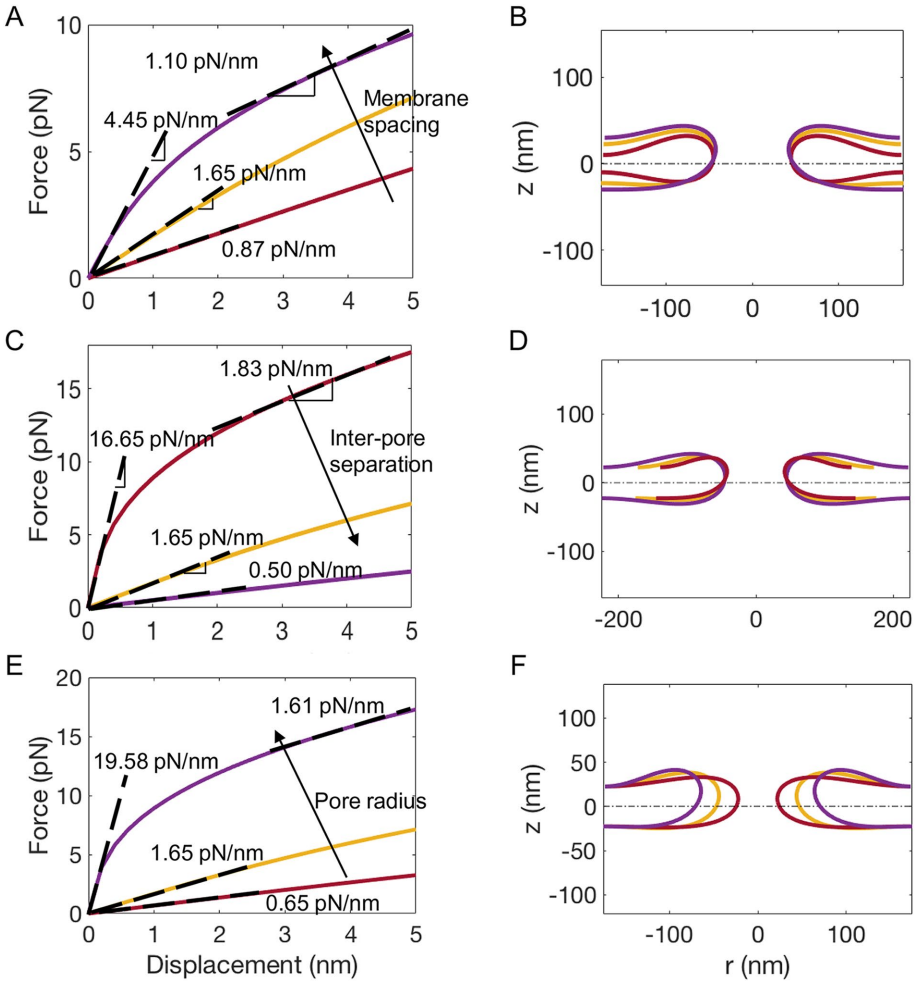

FIGURE 5: Effect of geometry on the mechanical response of the two-membrane system. (A) Force-displacement plots of the two-membrane system, depicted in Figure 3A, but at bilayer separations of 60 nm (purple curve), 45 nm (yellow curve), and 20 nm (red curve). (B) The calculated geometry of the three systems at a displacement of 5 nm (color coding as in A). (C) Force-displacement plots of the two-membrane system as in Figure 3A, but with outer radii of ~220 nm (purple curve), 175 nm (yellow curve), and ~140 nm (red curve). (D) The geometry of the three systems corresponding to a displacement of 5 nm (color coding as in C). (E) Force-displacement plots of the two-membrane system as in Figure 3A, but with pore radii of 67.5 nm (purple curve), 45 nm (yellow curve), and 22.5 nm (red curve). (F) The geometry of the three systems corresponding to a displacement of 5 nm (color coding as in E). The effective flexural stiffnesses at low and high displacements are labeled on the plots in A, C, and E.

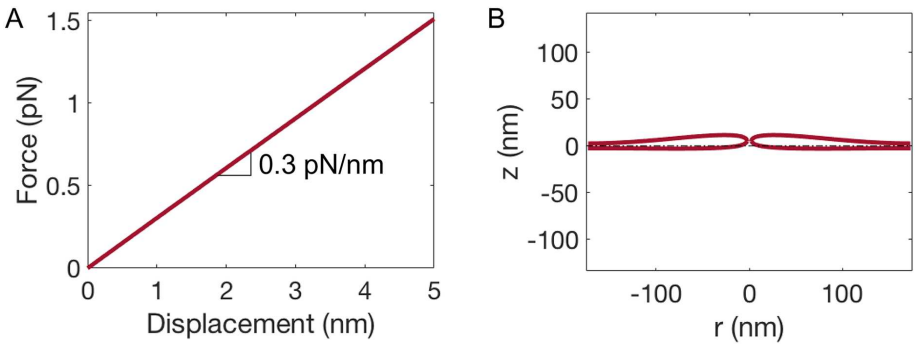

FIGURE 6: Mechanical response of the two-membrane patch at vanishing membrane spacing and pore radius. (A) Force-displacement plot shows a flexural stiffness of 0.3 pN/nm, which is nearly two times the stiffness of a single membrane. (B) The geometry of the membranes corresponding to a displacement of 5 nm.

(Figure 6A), which is about 2.3 times the stiffness of a single membrane (0.13 pN/nm). Figure 6B shows the geometry of such a structure. These results validate our double-membrane calculations and also confirm the assumption of other authors (Vaziri *et al.*, 2006) that the double-membrane system should have twice the stiffness of the single-membrane system when the two membranes have zero membrane spacing.

DISCUSSION

In this paper, we calculated the flexural stiffness of the nuclear envelope with a computational model that accounted for its geometry. The calculations revealed that for the assumed geometry and boundary conditions, the envelope is much stiffer than has been previously assumed. The bending modulus is an order of magnitude higher than that of a single membrane (Figure 4 and Table 1) and approximately five times higher than the estimated bending modulus of the mammalian nuclear lamina (Table 1).

The flexural stiffness of the nuclear envelope was significantly larger at higher spacings between the adjacent membranes (Figure 5), which suggests that a key reason for the increased flexural stiffness is the fact that the membranes are spaced apart from each other. In contrast to membranes that are close to each other, forces acting in the plane of membranes that are farther apart generate higher moments around the curved plane about which the membranes bend. For the same deformation, the in-plane forces produce larger moments, enabling the membranes to support larger moments. This is similar to the classic example of an I-beam structure that is designed to maximize its flexural stiffness. In an I-shape, material is arranged away from the middle of the cross-sectional plane about which the I-beam bends, resulting in a larger moment of inertia and hence larger effective flexural stiffness compared with a beam without the I-cross-section. Nuclear membranes in a way, are a 2D analogue of the same design principle. Confirming this concept, the flexural stiffness of the double-membrane system approached a value that is twice that of a single membrane when the membrane spacing and the pore diameter were reduced to minimum values.

Our model did not account for linkages between nesprins and SUN proteins, which are embedded in the ONM and INM, respectively (Tapley and Starr, 2013; Cain *et al.*, 2014). Linkages between them may reinforce the envelope against applied mechanical stresses (Agrawal and Lele, 2019). Also, the LINC complex transmits mechanical stresses

to the envelope that could modulate the in-plane tension in the envelope, thereby altering nuclear envelope bending. It is therefore possible that the envelope may be stiffer than our estimate here, particularly in cells that contain an intact LINC complex. Likewise, nuclear pore complexes may also contribute to the stiffness of the nuclear envelope, as the NPC is deformable (Deviri *et al.*, 2019).

Our results suggest that the nuclear envelope is in principle capable of balancing significant mechanical stresses even in cell types containing the nuclear lamina and may be important in determining nuclear response to cellular stresses. This is roughly consistent with a previous study that the mechanics of the nuclear membrane is required for explaining the deformation behavior of the nucleus under indentation (Vaziri *et al.*, 2006). However, our calculations do not account for key effects that could potentially make the envelope softer than our theoretical estimates here. For example, our assumed geometry of a uniform separation between the ONM and the INM may not be generally true but applicable only in some regions for a given nucleus. Indeed, substantial waviness in the ONM is commonly seen in electron micrographs of the envelope (e.g., see Figure 6F in Crisp *et al.*, 2006). The pore radius also may not be exactly what we have assumed (Deviri *et al.*, 2017), and furthermore, the assumed interpore separation may be spatially inhomogeneous for a given nucleus. Also, the envelope itself may be substantially bent in cells in high-curvature regions of the nucleus. The presence of a pressure differential across the nuclear envelope can generate additional tension in the membranes and stiffen the membrane against bending. However, if the pressure differential across the nuclear envelope reduces the membrane spacing, the nuclear envelope may become softer. All these parameters can profoundly impact the flexural stiffness. Our assumed boundary conditions need not be obeyed in cells; how the membranes behave mechanically, for example, at the pore is not known.

In summary, we estimated the bending modulus of the nuclear envelope by explicitly accounting for its geometry. Our calculations support the possibility of a spatial distribution of flexural stiffness even in the same nucleus caused by spatial variations in geometry and mechanical environment of the envelope. Our future studies will focus on how envelope proteins that link the membranes to the nuclear lamina and chromatin, and the membranes to the cytoskeleton, modulate envelope stiffness.

METHODS

Model

We modeled a membrane patch as a homogeneous 2D elastic surface that resists bending deformations. The internal energy of the membrane is defined by the Helfrich–Canham energy (Canham, 1970; Helfrich, 1973; Jenkins, 1977; Steigmann, 1999):

$$W = kH^2 + \bar{k}K \tag{1}$$

where H is the mean curvature, K is the Gaussian curvature, and k, $\bar{k}$ are the bending moduli. We consider the membrane to be inextensible and impermeable and define an augmented energy functional with membrane tension and transmembrane pressure as Lagrange multiplier fields. The equilibrium configurations then render stationary the potential energy and satisfy the Euler–Lagrange equation (Agrawal and Steigmann, 2009a,b),

$$k\left[\Delta H + 2H\left(H^2 - K\right)\right] - 2\lambda H = p \tag{2}$$

Here, ΔH is the surface Laplacian of the mean curvature, λ is the membrane tension, and p is the pressure across the membrane.

Computational model

To calculate the full nonlinear solution numerically, we solved the nonlinear Euler–Lagrange equation 3. In this generalized approach, the equations that define the geometry and the equilibrium conditions include (Agrawal and Steigmann, 2009a,b)

$$r'(s) = \cos\psi,\ z'(s) = \sin\psi,\ \psi' = 2H - \sin\psi/r,\ H' = L/r,$$

$$\text{and } L' = r\left[\left(\frac{2\lambda}{k}\right)H - 2H\left(H - \sin\frac{\psi}{r}\right)^2\right] \tag{3}$$

where r is the radial distance from the axis of revolution, z is the height, ψ is the angle the outward normal vector at a boundary makes with the radial vector, and L is the transverse force (along the surface normal) that the membrane experiences at a boundary. The pressure across the membrane was set to zero. The tension is assumed to be constant in the membrane, which means that the area of the domain between adjacent pores is not conserved. Changes in the area are assumed to be made possible through exchange of lipids between the nuclear envelope and the endoplasmic reticulum. We note that these are equilibrium calculations, and so we do not simulate lipid exchange, but rather calculate the final structure under force. The geometric quantities and the boundary conditions for the single-membrane and double-membrane systems are shown in Figures 2, A and B, and 3, A and B, respectively. We integrated the equations numerically in Matlab using the BVP4C solver subject to the boundary conditions discussed above for the linear system.

Mechanics of a single membrane

For purposes of comparison with the full model, here we examine a single-membrane patch with no pore in it and an upward point force at its center. We employ the Monge representation to model the single membrane and assume that the gradients of membrane height of all order are small. As such, their products can be neglected. Then $H = 1/2\,\Delta z$ and $K = 0$, and the equilibrium equation 2 can be linearized to obtain

$$\frac{1}{2}k\left[\Delta(\Delta z)\right] - \lambda\Delta z = p \tag{4}$$

where Δ is the Laplacian evaluated on the projected plane (Agrawal and Steigmann, 2009a).

We apply upward-acting point forces and compute the deflection profile (Figure 2, A and B). We assume that both the membrane tension and the pressure across the membrane are zero. We further assume that the membrane shape possesses rotational symmetry about the vertical axis passing through the center of the pore. For this case, the equilibrium equation further simplifies to $\Delta(\Delta z) = 0$, whose solution is (Ventsel and Krauthammer, 2001)

$$z(r) = c_1 \ln r + c_2 r^2 \ln r + c_3 r^2 + c_4 \tag{5}$$

For the membrane with no pore, we assume that the membrane patch has zero slope and the vertical force at the pole is equal to the applied force (at $r = 0$) (Figure 2A). We assume that the membrane has zero height and zero slope at the far boundary ($r = b$).

Applying the boundary conditions yields the solution

$$z(r) = \frac{F}{4\pi k}\left[\frac{(b^2 - r^2)}{2} + r^2 \ln\left(\frac{r}{b}\right)\right] \tag{6}$$

The maximum deflection occurs at the inner rim and is given by

$$z_{max} = z(0) = \frac{F}{4\pi k}\left[\frac{(b^2)}{2}\right] \tag{7}$$

To extract the effective flexural stiffness for the single membrane, we rearrange the above solution as

$$F = \left(\frac{k}{\beta}\right) z_{max} = k_s z_{max} \quad (8)$$

where

$$\beta = \frac{1}{4\pi}\left[\frac{(b^2)}{2}\right] \quad (9)$$

$k_s = \frac{k}{\beta}$ is the effective bending stiffness of the membrane and determines the maximum extent to which the membrane deforms when subjected to a point force F. It is important to note that while k is a material property, β is purely a geometric parameter determined by the outer radius of the membrane patch.

For the membrane with a pore, we assume the same boundary conditions at the far boundary. At the point of force application ($r = \alpha$), we assume that the membrane patch has zero moment and the vertical force is equal to the applied force (Figure 2B).

Applying the boundary conditions yields the solution

$$z(r) = \frac{F}{4\pi k}\left[a^2(1-\alpha+2\ln a)\ln\left(\frac{a}{r}\right)+r^2\ln r - a^2\ln a+\frac{\alpha}{2}(a^2-r^2)\right] \quad (10)$$

The maximum deflection occurs at the inner boundary where

$$F = \left(\frac{k}{\beta_h}\right) z_{max} = k_h z_{max} \quad (11)$$

Above, $F = 2\pi a f$ and

$$\beta_h = \frac{1}{4\pi}\left[a^2(1-\alpha+2\ln a)\ln\left(\frac{a}{b}\right)+b^2\ln b - a^2\ln a+\frac{\alpha}{2}(a^2-b^2)\right] \quad (12)$$

ACKNOWLEDGMENTS

This work was supported by National Science Foundation Grants no. CMMI 1562043 and CMMI 1727271 (A.A.) and by National Institutes of Health U01 CA225566 and NIH R01 EB014869 (T.P.L.).

REFERENCES

Agrawal A (2011). Mechanics of membrane–membrane adhesion. Math Mech Solids 16, 872–886.

Agrawal A, Lele TP (2019). Mechanicsof nuclear membranes. J Cell Sci 132, jcs229245.

Agrawal A, Steigmann D (2009a). Boundary-value problems in the theory of lipid membranes. Continuum Mech Thermodyn 21, 57–82.

Agrawal A, Steigmann D (2009b). Modeling protein-mediated morphology in biomembranes. Biomech Model Mechanobiol 8, 371–379.

Belgareh N, Doye V (1997). Dynamics of nuclear pore distribution in nucleoporin mutant yeast cells. J Cell Biol 136, 747–759.

Bermúdez H, Hammer DA, Discher DE (2004). Effect of bilayer thickness on membrane bending rigidity. Langmuir 20, 540–543.

Boal D, Boal D (2012). Mechanics of the Cell, Cambridge: Cambridge University Press.

Cain NE, Tapley EC, McDonald KL, Cain BM, Starr DA (2014). The SUN protein UNC-84 is required only in force-bearing cells to maintain nuclear envelope architecture. J Cell Biol 206, 163–172.

Canham PB (1970). The minimum energy of bending as a possible explanation of the biconcave shape of the human red blood cell. J Theor Biol 26, 61–81.

Crisp M, Liu Q, Roux K, Rattner JB, Shanahan C, Burke B, Stahl PD, Hodzic D (2006). Coupling of the nucleus and cytoplasm: role of the LINC complex. J Cell Biol 172, 41–53.

D'Angelo MA, Anderson DJ, Richard E, Hetzer MW (2006). Nuclear pores form de novo from both sides of the nuclear envelope. Science 312, 440–443.

Denais CM, Gilbert RM, Isermann P, McGregor AL, te Lindert M, Weigelin B, Davidson PM, Friedl P, Wolf K, Lammerding J (2016). Nuclear envelope rupture and repair during cancer cell migration. Science 352, 353–358.

Deserno M, Müller MM, Guven J (2007). Contact lines for fluid surface adhesion. Phys Rev E 76, 011605.

Deviri D, Discher DE, Safran SA (2017). Rupture dynamics and chromatin herniation in deformed nuclei. Biophys J 113, 1060–1071.

Deviri D, Pfeifer CR, Dooling LJ, Ivanovska IL, Discher DE, Safran SA (2019). Scaling laws indicate distinct nucleation mechanisms of holes in the nuclear lamina. Nat Phys 15, 823–829.

Dultz E, Ellenberg J (2010). Live imaging of single nuclear pores reveals unique assembly kinetics and mechanism in interphase. J Cell Biol 191, 15–22.

Franke WW, Scheer U, Krohne G, Jarasch ED (1981). The nuclear envelope and the architecture of the nuclear periphery. J Cell Biol 91, 39s–50s.

Halfmann CT, Sears RM, Katiyar A, Busselman BW, Aman LK, Zhang Q, O'Bryan CS, Angelini TE, Lele TP, Roux KJ (2019). Repair of nuclear ruptures requires barrier-to-autointegration factor. J Cell Biol 218, 2136–2149.

Helfrich W (1973). Elastic properties of lipid bilayers: theory and possible experiments. Z Naturforsch C 28, 693–703.

Jenkins J (1977). Equations of mechanical equilibrium of a model membrane. SIAM J Appl Math 32, 755–764.

Landau LD, Lifshitz EM (1986). Theory of Elasticity, Oxford, UK: Butterworth-Heinemann.

Lim HWG, Huber G, Torii Y, Hirata A, Miller J, Sazer S (2007). Vesicle-like biomechanics governs important aspects of nuclear geometry in fission yeast. PLoS One 2, e948.

Ogawa-Goto K, Tanaka K, Gibson W, Moriishi E, Miura Y, Kurata T, Irie S, Sata T (2003). Microtubule network facilitates nuclear targeting of human cytomegalovirus capsid. J Virol 77, 8541–8547.

Otsuka S, Bui KH, Schorb M, Hossain MJ, Politi AZ, Koch B, Eltsov M, Beck M, Ellenberg J (2016). Nuclear pore assembly proceeds by an inside-out extrusion of the nuclear envelope. eLife 5, e19071.

Steigmann D (1999). Fluid films with curvature elasticity. Arch Ration Mech Anal 150, 127–152.

Tapley EC, Starr DA (2013). Connecting the nucleus to the cytoskeleton by SUN-KASH bridges across the nuclear envelope. Curr Opin Cell Biol 25, 57–62.

Torbati M, Lele TP, Agrawal A (2016). Ultradonut topology of the nuclear envelope. Proc Natl Acad Sci USA 113, 11094–11099.

Tran PT, Marsh L, Doye V, Inoue S, Chang F (2001). A mechanism for nuclear positioning in fission yeast based on microtubule pushing. J Cell Biol 153, 397–411.

Vaziri A, Lee H, Mofrad M (2006). Deformation of the cell nucleus under indentation: mechanics and mechanisms. J Mater Res 21, 2126–2135.

Vaziri A, Mofrad MR (2007). Mechanics and deformation of the nucleus in micropipette aspiration experiment. J Biomech 40, 2053–2062.

Ventsel E, Krauthammer T (2001). Thin Plates and Shells: Theory, Analysis, and Applications, New York: Marcel Dekker.

Warecki B, Ling X, Bast I, Sullivan W (2020). ESCRT-III-mediated membrane fusion drives chromosome fragments through nuclear envelope channels. J Cell Biol 219, e201905091.

West RR, Vaisberg EV, Ding R, Nurse P, McIntosh JR (1998). cut11(+): a gene required for cell cycle-dependent spindle pole body anchoring in the nuclear envelope and bipolar spindle formation in Schizosaccharomyces pombe. Mol Biol Cell 9, 2839–2855.

Yi X, Shi X, Gao H (2011). Cellular uptake of elastic nanoparticles. Phys Rev Lett 107, 098101.

Zheng L, Schwartz C, Magidson V, Khodjakov A, Oliferenko S (2007). The spindle pole bodies facilitate nuclear envelope division during closed mitosis in fission yeast. PLoS Biol 5, e170.